Dynamical modeling of bi-layer Aluminium adhesive tape for laser shock applications

M. Ayad, S. Ünaldi, M. Scius-Bertrand, C. Le Bras, B. Fayolle, L. Berthe

Optics & Laser Technology 163 (2023) 109366

Contents lists available at ScienceDirect

Optics and Laser Technology

journal homepage: www.elsevier.com/locate/optlastec

Dynamical modeling of bi-layer Aluminium adhesive tape for laser shock applications

M. Ayad [a], S. Ünaldi [a], M. Scius-Bertrand [b], C. Le Bras [c], B. Fayolle [a], L. Berthe [a,*]

[a] PIMM, UMR8006 ENSAM, CNRS, CNAM, 151 bd de l'Hôpital, 75013 Paris, France
[b] Rescoll, 8 All. Geoffroy Saint-Hilaire, 33600 Pessac, France
[c] CEA CESTA, 15 avenue des Sablières CS60001, Le Barp Cedex 33116, France

ARTICLE INFO

Keywords:
Laser shock
Dynamic material characterization
Polymer glassy behavior
High strain rate
Johnson–Cook
Steinberg–Cochran–Guinan

ABSTRACT

The presented work covers the response of Aluminium tape (Al tape) under high strain rate of deformation (order of 10^6 s^{-1}) using laser shock. High power laser (J) with a short pulse duration (ns) is used to create laser shock within the water confinement regime on two Al tape configurations in order to apply low and high pressure (order of MPa and GPa). Al tape has been modeled using Johnson-Cook (J-C) material model for the Al layer, and Steinberg–Cochran–Guinan (SCG) material model (elastic with pressure dependence) for the adhesive layer, both material models are coupled with Grüneisen equation of state. The Al tape model has been validated by comparing the simulated Back Face Velocity (BFV) of the target with the measured one by the Velocity Interferometer System for Any Reflector (VISAR). In addition, the validated material model is used to conduct the sensitivity studies about the transmitted pressure depending on the acoustical impedance of the target and adhesive thickness. Moreover, location and magnitude of maximum tensile stress within the target are calculated in function of the adhesive thickness of the Al tape. Finally, it has been proved that using one laser beam configuration, maximum tensile zone could appears close to the front face by increasing the adhesive thickness.

1. Introduction

Laser based processes are widely investigated during the last decades in the aeronautics industry and consequently for the structural parts. Laser Shock Peening (LSP) is one of the most used and investigated process on metallic structures to enhance their properties, to extend their lifetime and modify their microstructure properties [1–7]. Although during LSP process, a protective layer should be used to protect the target from created thermal effects due to the usage of laser [8,9]. The second mostly used process is the LAser Shock Adhesion Test (LASAT) [10,11], where the shock wave generated by the laser is used to determine the bonding strength of joints in composite laminates [10,12]. In order to be able to localize the shock wave effects, one should know the loading created by the laser and the material behavior of the target under laser shock. Laser Paint Stripping Process (LPSP) also can be mentioned [13], where the generated shock wave by the laser is used to remove the paint from the aluminium substrate. The authors managed to remove paint from aluminium substrate by applying the laser from the aluminium side. For industrial purposes, protective layer can be used for the paint sided laser applications to reduce the ablative effects of the laser. Therefore, for laser shock applications, a protective layer should be used either on metals (LSP) or on polymers (LASAT or LPSP).

The pressure which is induced by laser pulse has been studied and characterized on aluminium surface by Scius-Bertrand et al. [14]. The authors used 1D ESTHER code [15] to provide ablation pressure created by water confined laser and validated on different laser configurations and facilities. Very recently, Ayad et al. used the provided scaling laws from Scius-Bertrand et al. [14] counting the rarefaction phenomena described by Rondepierre et al. [16] to simulate the 2D phenomena appeared under laser shock, and validate theirs numerical studies by experimental laser shock experiments [17]. Hereby, ablation pressure created by laser shock has been well studied and characterized on aluminium targets. Therefore, the ablative layer we want to use to protect the sample from the thermal affect should have aluminium on the top face. The other face of this layer should be an adhesive to ensure the adhesion with the target. In her PhD (pages 134–139), Scius-Bertrand showed that the transmitted pressure to the target by an aluminium tape was sensitively different from the ablation pressure profile applied on the front face of the tape [18]. It is then required

* Corresponding author.
E-mail addresses: mohamaddayadd@gmail.com (M. Ayad), laurent.berthe@cnrs.fr (L. Berthe).

https://doi.org/10.1016/j.optlastec.2023.109366
Received 30 December 2022; Received in revised form 19 February 2023; Accepted 8 March 2023
Available online 20 March 2023

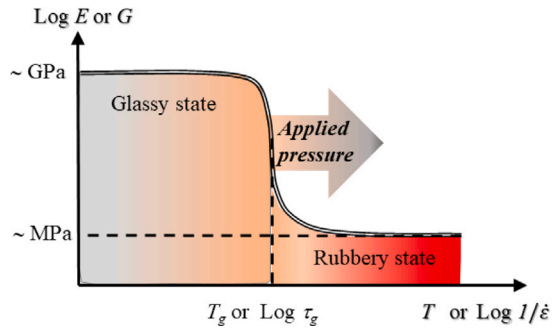

Fig. 1. Tensile or shear modulus as a function of applied temperature (T) or strain rate ($\dot{\varepsilon}$), influence of applied pressure on glass transition or frontier between glassy state and rubbery state. T_g and τ_g are the glass transition in terms of temperature and characteristic time respectively.

to either extract the transmitted pressure and apply it on the target or apply the ablation pressure on the entire stack (Al tape with the target).

In order to analyze the influence of using a protective layer during LSP process, one should know what is transmitted to the target during the laser shock process. Bovid et al. calculated the transmitted pressure from the applied overlays to the substrate during the LSP process [19]. The authors prove that the usage of opaque overlays provide up to 50% increases in the pressure magnitude based on experimental results on 7085 aluminium alloy and Ti-6Al-4V. Nonetheless, the authors based on the maximum peak of the velocity profile to validate his formulation for opaque overlay pressure predictions. The authors simulated their dynamic problem by imposing initial velocity to the Al tape, and by using static mechanical properties as shear modulus for their polymers (polyrubber and neoprene) without any strain rate sensitivity. Peyre et al. discussed impedance mismatching, and proved that applied stress on steel could be increased by 50% with the usage of Al coating [20]. Hong et al. proved that the black paint on the target can improve the amplitude of induced shock wave, by comparing the maximum pressure of the shock wave induced on the target with and without the black paint overlay for different confining materials [21].

In order to obtain precise modeling, the energy dissipation through this tape should be identified. Due to the high strain rate of deformation [17] induced by laser shock, elastomers could subject a glass transition or α transition which leads to a glassy state [22]. This transition is strain rate dependent where it can be observed at room temperature for high strain rate [23,24]. Very recently, Le Bras et al. studied the dynamic glass transition of Polycarbonate and Poydimethylsiloxane under laser shock. The authors show that dynamic glass transition in the polymers that induce significant behavior modifications, they used numerical and experimental laser shock coupled with Dielectric Relaxation Spectroscopy (DRS) measurements to identify the limit of the rubbery and glassy behavior of polymers under high pressure and strain rate [25]. Despite the strain rate dependency of the polymers, Mulliken and Boyce used three-dimensional rate-, temperature-, and pressure-dependent model to model the transition of yield behavior over wide range of temperatures (−140 °C to 180 °C) and strain rates (10^{-3} s^{-1} to 4000 s^{-1}).

As shown in Fig. 1, the shift in the glass transition is not only due to the high strain rate of the laser shock process, but also due to the increase in the applied pressure. This influence of pressure has been highlighted by Le Bras et al. to explain the mechanical response of polymers used as solid confinement under LSP conditions [25]. As a result, materials such as acrylic that are under static conditions in the rubbery state end up in the glassy state under conditions of high strain rate and pressure.

Since the ablative layer is required by multi-processes (LSP, LASAT and LPSP) where the micro and macro waves propagation are mandatory, the different layers of the tape should be modeled. Up to now, neither experiment nor simulation have been done to model the glassy behavior of acrylic in Al tape taking into account the pressure dependent criterion under high strain rate.

In the current work, the accurate methodology from Ayad et al. [17] has been used to characterize the adhesive layer under high strain rate produced by laser shock. First, experimental set-up is described. The experiments have been performed at the Héphaïstos Laser facility located in the PIMM laboratory (Procédés et Ingénierie en Mécanique et Matériaux), Paris, France and reproduced in the Monarque laser facility of Rescoll, Bordeaux, France (Section 2). Numerical model of the Al tape under high strain rate is presented in Section 3, which will be validated using the experimental results in Section 4. The validated material model will be used to make different sensitivity studies dedicated for LSP, LASAT and LPSP communities in Section 5. The obtained results are discussed in Section 6. Finally, conclusion and outlook are given in Section 7.

2. Experimental tools

The different experimental set-ups are used in two different laser facilities which are explained below. The very same Velocity Interferometer System for Any Reflector (VISAR) diagnostic is used for both experimental sets. After the explanation of each facility, the VISAR diagnostic description is given in details as well.

2.1. Héphaïstos

The majority of the experiments were conducted at Héphaïstos facility, PIMM lab, Paris, France. The laser used for the experiments is a Gaïa HP laser from THALES company, France. It is a flashlamp-pumped Nd:YAG with a Gaussian temporal profile. The laser can produce 14 Joules of energy, from two beams/channels in total with 7 ns of pulse duration (at Full Width Half Maximum, FWHM) and 2 Hz of repetition rate at wavelength of 532 nm. The energy output from the laser can be modified/controlled via software in the control room. The software consists of 3 main functions: Channel control, burst parameters and burst mode. However, the energy output given from the software is not the exact value due to beam losses while beam transportation and optics that is why energy measurement is done shot by shot and calibrated before each set of experiment using a calorimeter (QE50LP-H-MB-QED, Gentec, Québec, QC, Canada). The used focal spot is 4 mm diameter as shown in Fig. 2a.

2.2. Monarque

Some of the experiments were done at Monarque facility at RESCOLL, Pessac, France. The platform is composed of two Rhéa lasers from THALES company. They are based on the same technology as the Gaia lasers (flashlamp-pumped Nd:YAG with a Gaussian temporal profile), with the same wavelength (532 nm) and a total energy up to 10 Joules but a slightly shorter pulse duration (5 ns FWHM). The 5 Hz repetition rate combined with the automated displacement of the sample using a Kuka KR 50 R2100 robot enable the treatment of large surfaces (about 1 m^2) . The laser beams are first recombined and then separated using a polarizer, leading to the possibility of focusing all the energy in one face of the sample (mono-pulse configuration) or to focus half on each side of the sample (symmetric configuration). The energy delivered by the lasers is calibrated using the same calorimeter as at Héphaïstos facility and the spatial distribution of the energy is ensured to be homogeneous using DOE as shown in Fig. 2b.

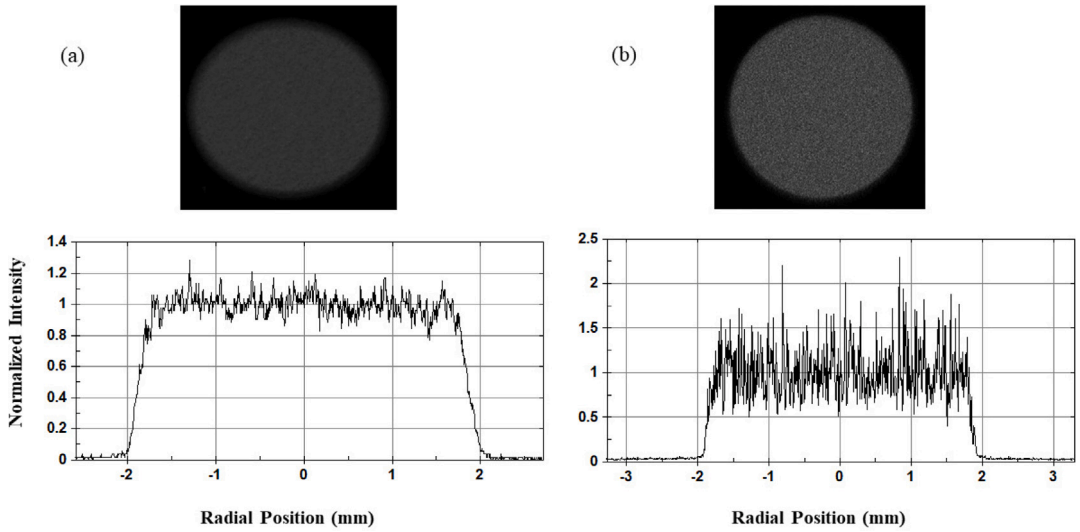

Fig. 2. CCD image of a 4 mm focal spot from two different laser platform Héphaïstos and Monarque in (a) and (b) accordingly.

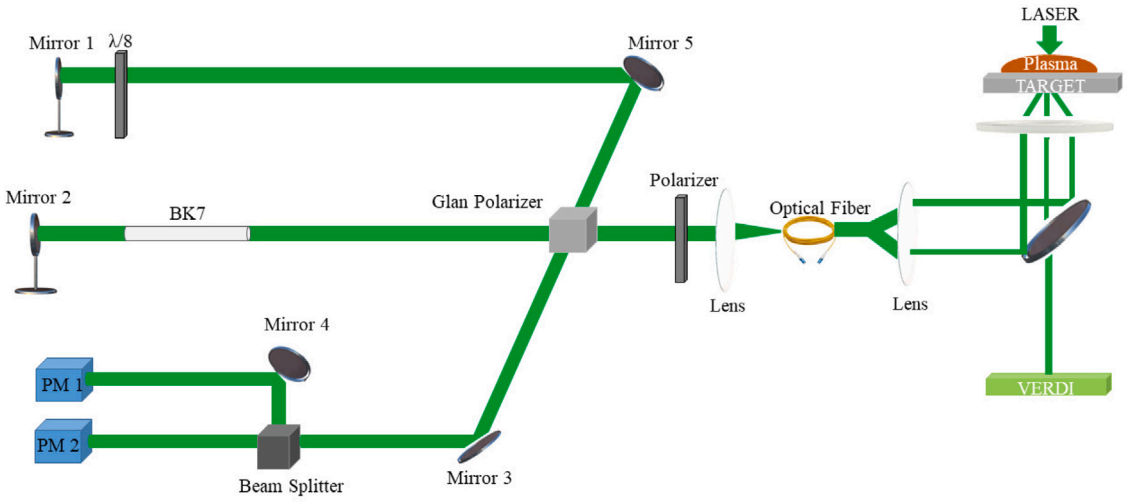

Fig. 3. Probe Part and Interferometer Part of the VISAR set up.

2.3. VISAR diagnostic

Due to the high strain rate produced by laser shock (order of 10^6 s^{-1}); experimental measurements are performed using a VISAR system. By applying the controlled laser on the front surface of the specimen, material response is extracted from the obtained back surface velocity. This velocity is measured via VISAR diagnostic which has a working principle of Michelson Interferometer [26,27]. The probe laser (532 nm) is reflected from the back face of the specimen which is already accelerated because of the applied shock wave. Then the created Doppler Shift is monitored [16]. With the help of the VISAR measurements, wave propagation within the targets can be monitored as function of velocity–time.

The VISAR set up consists of 2 main parts that are divided as Probe Part and Interferometer Part. In order to process the velocity measurements, the Doppler Shift of a mono mode probe laser (VERDI) is reflected at the rear surface as shown in Fig. 3.

Fig. 3 also shows the schematic representation for the interferometer part of the VISAR setup for the whole set of experiments. As one can see, the first arm is placed between the phase plate and the mirror M1 (reference branch at time t). In addition, the second arm is in between the glan polarizer and the mirror M2 (delayed branch at t-τ). This branch also contains a crystal to apply the delay τ to the signal. After that, the beam splitter receives two signals interfering at t and t-τ. Then, the mirror M4 guides the interference pattern into the sensors. The optical assembly formed by the polarizer P and the wave plate $\lambda/8$ enables the creation of two interference phase-shifted signals with a $\pi/2$. The information of these systems are respectively detected by the Photo multiplier 1 (PM1) and Photo multiplier 2 (PM2) via the beam splitter. The data obtained by the oscilloscope is transmitted to the computer. From the software, corresponding velocity profiles can be extracted.

3. Modeling

Laser shock is known by high strain rate of deformation (order of 10^6 s^{-1}), resulting from the high pressure (GPa) applied in (ns) pulse duration. Due to the high strain rate of deformation, physical

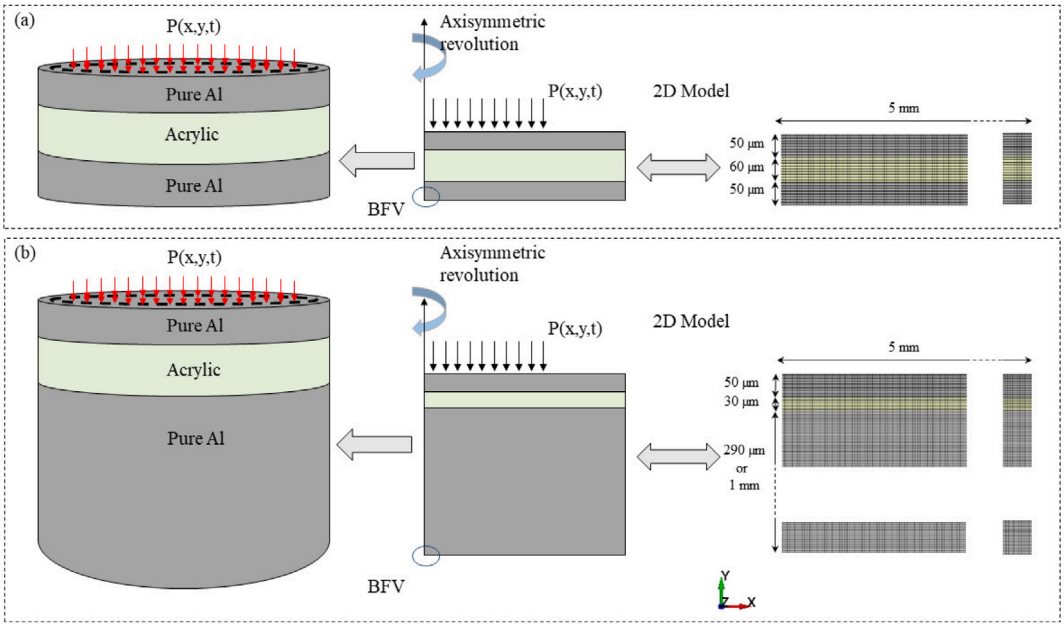

Fig. 4. 2D axisymmetric model for two configurations. (a) sample made of two aluminium tape, (b) made of aluminium tape attached on thicker Pure Al sample (290 µm and 1 mm).

phenomenons are difficult to measure and to analyze experimentally during the wave propagation. Therefore, numerical simulation is performed using LS-DYNA explicit solver to analyze and furthermore to optimize the laser process. The developed mesh and the used material model for Al and acrylic are shown in Section 3.1, coupled with Grüneisen equation of state. The shock created by the plasma is presented by an applied temporal and spatial profile as described below in Section 3.3.

3.1. Mesh and geometry

To simulate the shock wave propagation within the target, 2D axisymmetric model is used, with 5 µm × 2 µm mesh size in the target, and 5 µm × 1 µm in the Al tape due to its small thickness as shown in Fig. 4. In this study, two configurations of the Al tape under laser shock has been used. The first one is the folded Al tape as shown in Fig. 4a, and the second is the Al tape attached to thicker Pure Al sample (290 µm and 1 mm) as shown in Fig. 4b. The ratio of width to thickness has been taken large enough to prevent radial effects and reflection from the borders as the experimental case.

3.2. Material model

The modeling of dynamical laser shock process requires the strain rate sensitivity which is taken in account by using Johnson–Cook material model (Section 3.2.1) and coupled with Grüneisen equation of state (Section 3.2.3) for modeling the Pure Al. However the material model of the acrylic has been chosen to be elastic with pressure dependence, which can be modeled by using Steinberg material model (Section 3.2.2) also coupled with Grüneisen equation of state (Section 3.2.3).

3.2.1. Johnson–Cook material model

Following our previous works [17], Pure Al has been simulated using Johnson–Cook material model (MAT_015), which defines the plastic flow stress by taking into account the strain hardening modulus and exponent B and n accordingly, strain rate sensitivity C as noted in Eq. (1). Where the elastic limit will be calculated as function of the initial yield strength A, taking into account the strain rate sensitivity $(\dot{\bar{\varepsilon}}_p/\dot{\epsilon_0})$.

$$\bar{\sigma}_{eq} = \left(A + B\bar{\varepsilon}_p^{n}\right)\left(1 + C\ln\left(\frac{\dot{\bar{\varepsilon}}_p}{\dot{\epsilon}_0}\right)\right)\left(1 - \left(\frac{T - T_0}{T_m - T_0}\right)^{m}\right), \tag{1}$$

where $\bar{\varepsilon}_p$ is the equivalent plastic strain, m is the thermal softening coefficient.$\dot{\bar{\varepsilon}}_p$ and $\dot{\epsilon_0}$ are the plastic and the reference strain rate. T_0 and T_m are the room and melting temperature respectively.

3.2.2. Steinberg material model

Since the polymer behavior is "highly engineered pressure sensitive acrylic adhesive" as noted on the supplier website (www.3m.com), Steinberg–Cochran–Guinan (SCG) material model has been used to simulate the acrylic layer of the Al tape. The material type (MAT_011) takes into account the temperature and the pressure sensitivities for the elastic properties and the yield criterion [28]. In this study, the elastic part of the material model with the pressure dependence has been used, where the shear modulus G will be calculated as in Eq. (2).

$$G = G_0[1 + \beta_G P V^{1/3}], \tag{2}$$

where G_0 is the initial shear modulus which will increase with the increasing pressure P according to the pressure sensitivity parameter β_G (GPa^{-1}). This parameter is the ratio between shear modulus derivative with respect to pressure over the initial shear modulus ($\beta_G = \frac{1}{G_0}\frac{\partial G}{\partial P}$). V is the relative volume during the deformation under shock wave propagation.

3.2.3. Equation of state

Due to the high pressure applied on thin foils, it is necessary to couple the material model with an equation of state which is capable of relating the sudden pressure, internal energy and density changes during the shock wave propagation [29]. For this propose, Grüneisen equation of state as defined in LS-DYNA (EOS_GRUNEISEN) with cubic shock-velocity as a function of particle velocity $v_s(v_p)$ has been used. The pressure of material during compression and tension are defined in Eqs. (3a) and (3b) accordingly.

$$p = \frac{\rho_0 {C_0}^2 \beta[1 + (1 - \frac{\gamma_0}{2})\beta - \frac{a}{2}\beta^2]}{[1 - (S_1 - 1)\beta - S_2\frac{\beta^2}{\beta+1} - S_3\frac{\beta^3}{(\beta+1)^2}]^2} + (\gamma_0 + a\beta)E, \tag{3a}$$

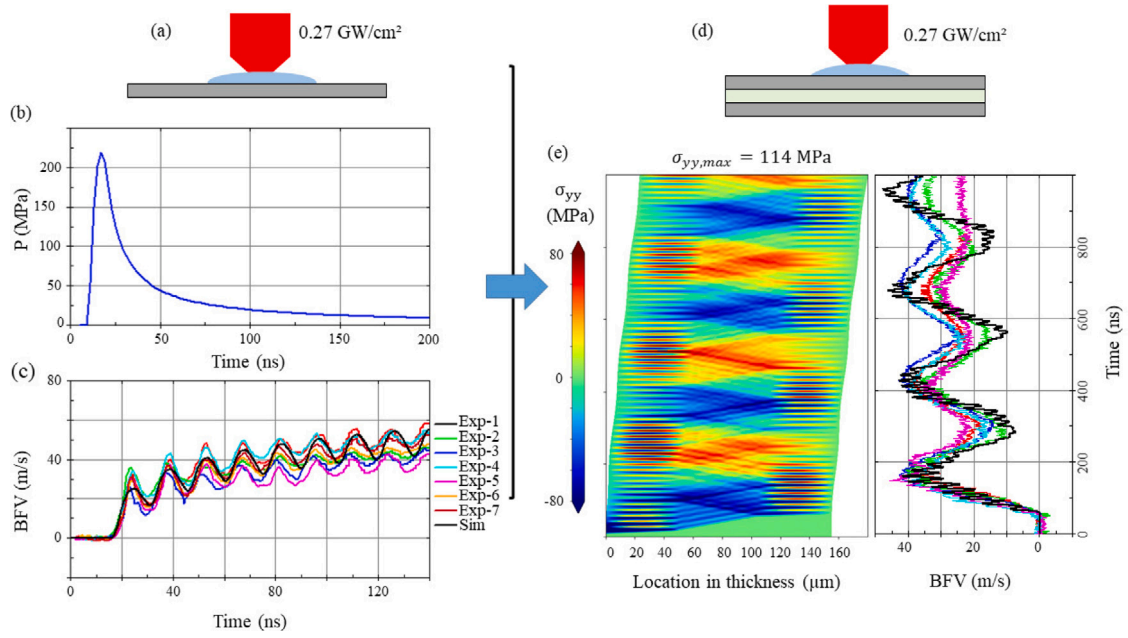

Fig. 5. Pure Al layer of the Al tape in (a) under laser shock, with the used pressure (b) to obtain the simulated BFV profile and compared with the experimental one (c). Folded Al tape in (d), with its response under laser shock in (e).

$$p = \rho_0 {C_0}^2 \beta + (\gamma_0 + a\beta)E, \tag{3b}$$

where C_0 is the initial shock velocity v_s for zero particle velocity v_p, and S_1, S_2 and S_3 are the unitless coefficients of the slope of the $v_s(v_p)$ curve. E denotes the internal energy, γ_0 is the unitless Grüneisen gamma and a its first order volume correction, $\beta = \frac{\rho}{\rho_0} - 1$.

3.3. Pressure loading modeling

As we mentioned before, the reason of using aluminium tape is the controlled and the well investigated pressure model produced by the created plasma on aluminium surface. In this section the spatial and temporal profile of the generated pressure are presented. As demonstrated in previous works, the combined approach presented by Scius-Bertrand [14] and Rondepierre [16] has been applied. And for the spatial laser intensity, the filtered profile of the measured one is applied, as discussed in previous work [17].

4. Results

In this section, two different configurations of Al tape has been modeled. The first one is the folded Al tape (Fig. 4a) under laser shock using the elastic part of SCG material model in Section 4.1. In order to be able to increase the power density on the aluminium tape, the second configuration of aluminium tape on thicker Pure Al target (290 µm and 1 mm) has been used as shown in Fig. 4b. For this configuration, the need of the pressure dependency will be elaborated.

4.1. Folded Al tape under laser shock

The first configuration of the Al tape (Fig. 4a) has been studied. For this sample, the acrylic layer of the Al tape has been modeled using the elastic part of SCG material model coupled with Grüneisen equation of state. The keys components of this simulation are the mechanical properties and equation of state constants. For this latter, C_0 is modified until the front of the shock wave arrives to the sample back face as the experimental one, S_1 and γ_0 are taken from literature works on dynamic simulation of epoxy polymer [30,31]. Density of the acrylic has been taken from online Ref. [32], while the shear modulus has been modified until the numerical model reproduce the experimental results. All these parameters are noted in Table 1.

Table 1
Mechanical and equation of state properties of the acrylic layer in the Al tape [30–32].

Material	ρ (kg/m^3)	G (MPa)	C_0	S_1	γ_0
Acrylic	1180	G	C_0	1.493	1.13

For this configuration, 0.27 GW/cm^2 laser intensity has been applied due to our measurement system's capability and fragility of the target. In order to be sure of the pressure generated by the plasma under this power density, same shock with same conditions on the Al layer of the tape after removing the acrylic with alcohol (Fig. 5a) has been applied. The 7 velocity signals (Exp-1...Exp-7) are plotted with the simulated one of the Pure Al which reproduce very well the experimental results (Fig. 5c), the used pressure profile is plotted in (Fig. 5b) with 220 MPa maximum pressure.

The obtained pressure profile in (Fig. 5b) is used to model the laser shock propagation into the folded Al tape (Fig. 5d). As shown in Fig. 5e, using G = 425 MPa, and C_0 = 1200 m/s the numerical model reproduces the experimental behavior of folded Al taped under high strain rate and 200 MPa pressure loading. The high value of shear modulus (equivalent to 1.2 GPa of elastic modulus) is in the range of Poly(methyl methacrylate) (PMMA) [33,34], due to the high strain rate regime of acrylic layer under shock, which has been found numerically around 5.9×10^6 s^{-1}. In order to analyze the origin of these peaks from the obtained velocity profiles, space–time diagram has been made of the axial stress propagation during the shock wave propagation as shown in Fig. 5e.

The blue color presents the compression waves generated by the plasma, which reflects into tensile waves (red color) while passing from Pure Al layer to acrylic layer (lower acoustic impedance), or meet the back face. The double taped Al tape has been modeled using the elastic part of SCG model under 0.27 GW/cm^2. Nonetheless, this sample could not handle higher power densities. Therefore, the Al tape has been

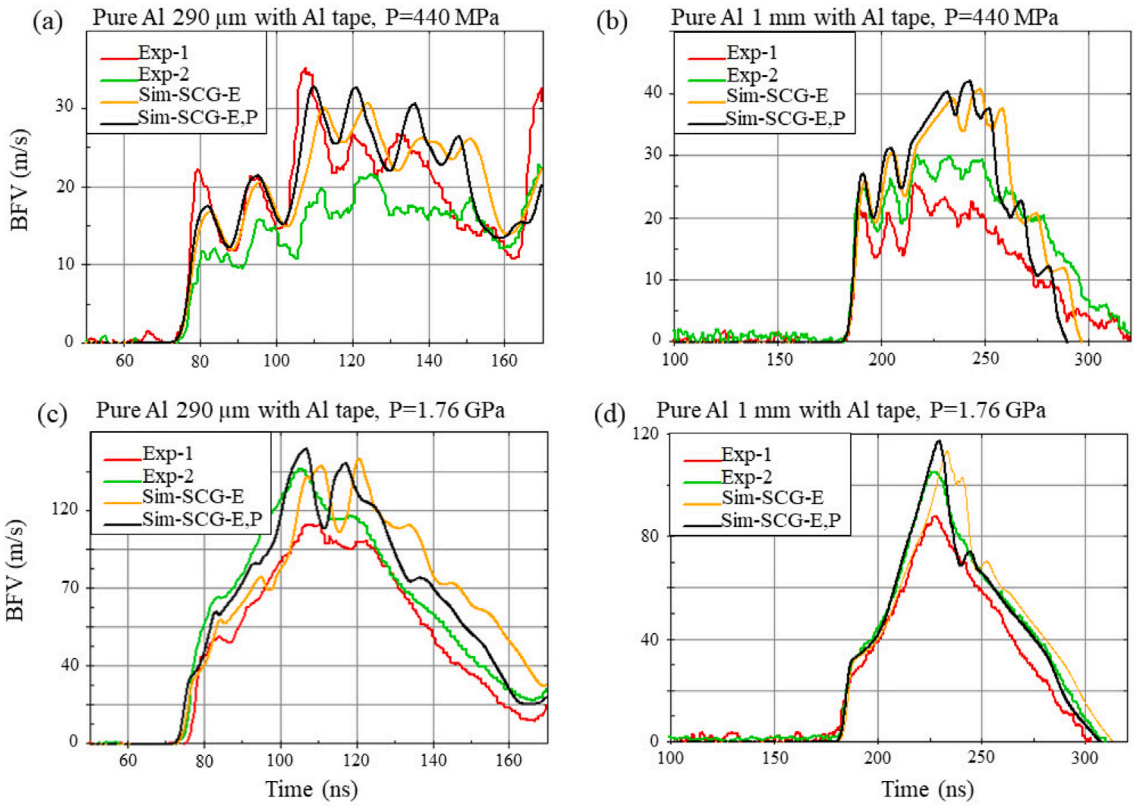

Fig. 6. Validation of the Simulated BFV for the taped Pure Al for two substrate thicknesses 290 µm and 1 mm in (a, c) and (b, d) accordingly. Where the experimental results are the red and green curves (Exp-1 & Exp-2), the numerical response of purely elastic material model is the gold curve (Sim-SCG-E) and the black one is the elastic with pressure dependence numerical results (Sim-SCG-E,P).

taped to a thick sample (290 µm and 1 mm), where higher power density could be applied to show the effect of pressure over the material response.

4.2. Simulation of folded Al tape under laser shock

In this section, the Al tape has been applied on thicker Al sample (290 µm and 1 mm) in order to increase the applied pressure on the aluminium tape. For this sample, elastic with pressure dependence in SCG material model is used. Pressure sensitivity parameter of the shear modulus (b) has been optimized until the numerical behavior reproduce the experimental behavior at low and high pressure. In Fig. 6, the numerical response of the sample 2 with two Al thickness (290 µm and 1 mm) with and without pressure dependency has been compared with the experimental measured BFV profile.

Fig. 6 shows a good correlation between the simulated BFV profile and the experimental results while taking into account the pressure sensitivity parameter ($\beta_G = 8$ GPa^{-1}), while the one simulated with ($\beta_G = 0$) needs a bigger shear modulus to fit the timing of the peaks and of the release (2.7 times higher than the used one G_0), but the shock wave will break out earlier than the experimental one. In addition, the simulated maximum velocity of the taped Al samples (290 µm and 1 mm) for pressure range from 660 MPa until 3.45 GPa has been compared with the experimental results as shown in Fig. 7.

In overall, the simulated maximum velocity (black triangle in Fig. 7) shows close values to the experimental results (Exp-1 & Exp-2) including 10% error bar. Moreover, a threshold of the interface bonding between the tape and the substrate has been used. The debonding threshold value of the stress at the tape interface with the substrate has been calibrated according to the numerous experiments that has been done, which has been found to be $\sigma_{yy,threshold} = 165$ MPa. This threshold has been modeled by adding Erosion criterion to one µm acrylic element at the interface with the substrate. The debonding of the tape has been observed by the period change of the shock wave after the first period, and has been proved by comparing the bonded assembly results (Sim-SCG-E,P) and the debonded one (Sim-SCG-E,P,Deb) with the experimental results in Fig. 8.

The numerical model of the Al tape with the debonding criteria (Sim-SCG-E,P,Deb) shows a perfect correlation with the experimental results for two different pressures 440 MPa and 1.76 GPa. The bonded simulation (Sim-SCG-E,P) propagates with bigger period as shown in Fig. 8a, while for the 1 mm Al substrate some peaks appeared (yellow curve) which does not exist in the experimental results. This can be seen more clearly under higher pressure on the taped 1 mm Pure Al. This debonding has been validated using the microscope after laser shock in PIMM laboratory.

5. Process optimization

The mismatching of acoustical impedance could change the ratio of transmitted pressure from the Al tape. Moreover, the delay of the shock wave propagation caused by the acrylic layer could change the maximum tensile zone produced in the substrate. In Section 5.1, Pure Al and Inconel-718 has been used to study the influence of Al tape on the transmitted pressure on the target, which is important for optimization of LSP for different acrylic thickness. Regarding the LASAT application, the acrylic thickness can be crucial since its thickness could change the localization of the maximum tensile zone which will be discussed in Section 5.2.

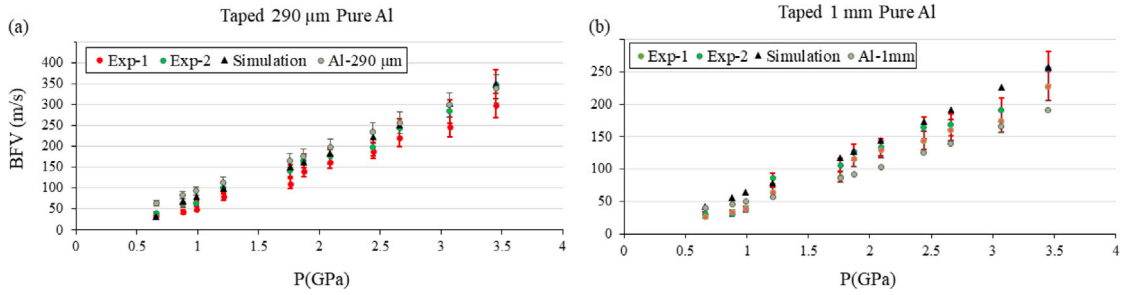

Fig. 7. Validation of the used numerical model for the taped Al of 290 μm and 1 mm in (a, c) and (b, d) accordingly.

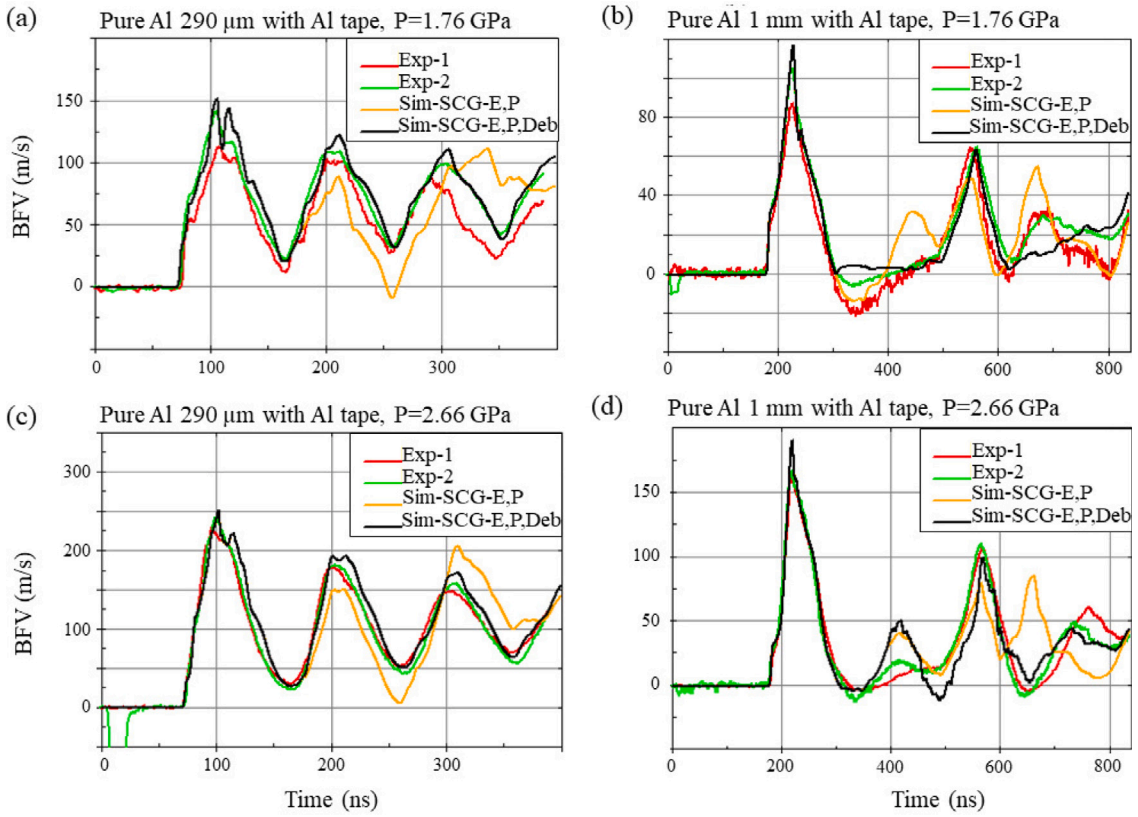

Fig. 8. Simulation of the shock wave propagation on the 290 μm and 1 mm taped Al samples in (a, c) and (b, d). Where the experimental results are the red and green curves (Exp-1 & Exp-2), the numerical response without the debonding criterion is the gold curve (Sim-SCG-E,P) while it is taken into consideration in the black one (Sim-SCG-E,P,Deb).

5.1. Transmitted pressure

The impedance mismatching could change the transmission factor of the pressure from the Al tape to the target (Pure Al and Inconel-718 alloy), J–C material model parameters of the Inconel 718 has been taken from Farahani et al. [35]. For Pure Al target, since the target is the same material as the first layer of the Al tape the transmitted pressure cannot be more than the applied one, where for the Inconel 718 alloy the transmitted pressure is bigger by 20% comparing to the applied one on the top of the Al tape as shown in Fig. 9a. In addition, for both metals the effect of acrylic thickness has been analyzed on the transmitted pressure in Fig. 9b, where the pressure is attenuated with big acrylic thickness.

5.2. Maximum tensile zone

With the used laser configuration for this study (mono-pulse), the maximum tensile zone within the target is usually close to the back free face. While the usage of Al tape changes the localization of the maximum tensile zone due to the delay in the acrylic layer and the reflection with the other layers. Therefore, the transmitted pressure has been calculated using the taped Pure Al of 1 mm thickness model using different acrylic thickness, and then applied on 1 mm Pure Al sample. Space–time diagrams has been generated to show the propagation of the stress waves through the target thickness, as shown in Fig. 10.

Fig. 10 depicts the stress propagation through target thickness for different acrylic thickness (26 μm, 50 μm, 80 μm, 110 μm, 140 μm and 200 μm accordingly in a, b, c, d, e, and f), where blue and red

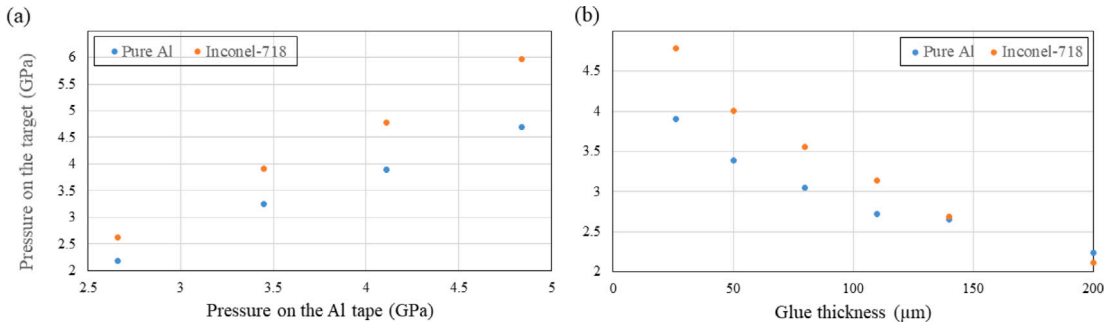

Fig. 9. Transmitted pressure to Pure Al (blue) and Inconel 718 alloy (orange) target top surface in function of the applied one on the Al tape and of acrylic thickness in (a) and (b) accordingly.

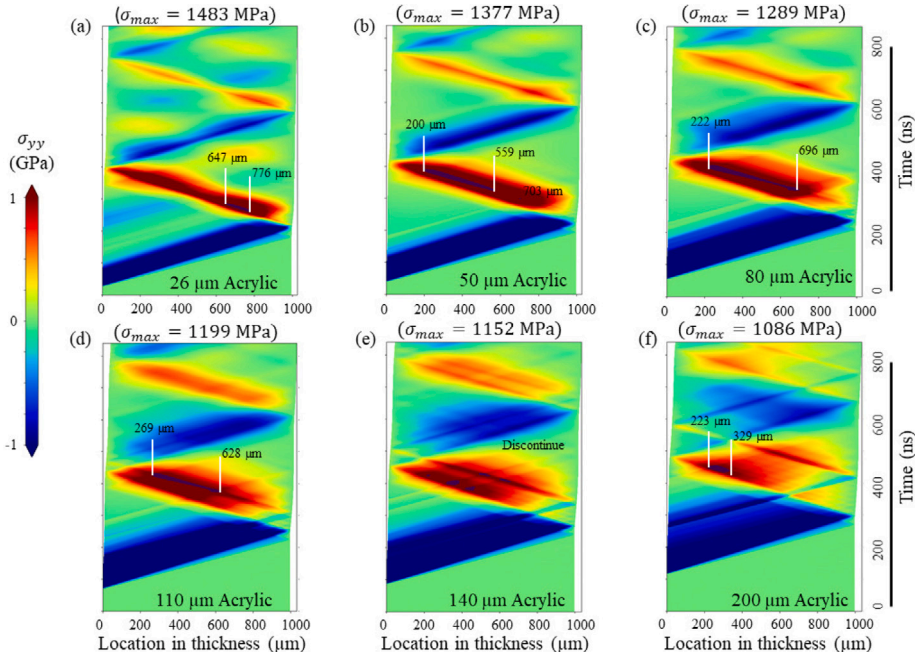

Fig. 10. Axial compression and tensile stress level σ_{yy} (blue and red colors respectively) during the wave propagation through the Pure Al sample (horizontal axis) and during the laser shock loading under 1.8 GW/cm^2 for different acrylic thickness(26 µm, 50 µm, 80 µm, 110 µm, 140 µm and 200 µm) in (a), (b), (c), (d), (e), and (f) accordingly.

colors represent the compression and tensile waves respectively. The maximum tensile stress level (GPa) has been colored by a black color in the 1 mm Pure Al target. As shown in this space–time diagrams, the tensile zone is approaching to the target front face and becoming more localized.

6. Discussion

The proper modeling of the polymer under high strain rate is of a crucial importance for the accurate characterization of the Al tape influence in laser shock process. Using Steinberg–Cochran–Guinan (SCG) coupled with Grüneisen equation of state for the acrylic layer, the numerical model reproduced the experimental results at two different laser shock platforms (Héphaïstos and Monarque).

Two different material configurations have been used as shown in Figs. 4a and 4b. The folded Al tape appeared to handle only 0.27 GW/cm^2 power density. While the second one which has been made of taped Al tape on 1 mm and 290 µm Pure Al samples handled higher pressure. The elastic part of the SCG material model (Sim-SCG-E) proves sufficient to reproduce the experimental results of the folded Al tape as shown in Fig. 5e, and also for the second configuration under low pressure as shown in Figs. 6a and 6b. While with the increasing of the applied pressure to 1.76 GPa, the elastic part of the SCG material model produce delayed wave comparing to the experimental results, as shows the gold curve in Figs. 6c and 6d. Therefore, the pressure dependence part of the material model (β_G parameter in Eq. (2)) has been optimized until the front, peak and the release waves meets the experimental ones (red and green curves), where a value of β_G = 8 GPa^{-1} is sufficient as shows the black curve (Sim-SCG-E,P) in Figs. 6c and 6d. Moreover, validation over all the experimental results has been done and the numerical model proves to reproduce the experimental peaks for both configurations (Fig. 4). The validation of the first peak velocity values with the experimental one is summarized in Fig. 7.

The validation of the material model consists also to validate the reflected waves (back and forth) not only the first peak of the BFV which has been done in Fig. 8. Therefore, debonding threshold has been

added to the Al tape connection with the substrate by adding erosion criterion to one μm of acrylic on the interface between the AL tape and the Pure Al substrate. Due to this debonding criterion, numerical model reproduce not only the first peak of the experimental ones but all other peaks times and magnitudes as shown in Fig. 8.

The validated material model has been used to make some sensitivity study about the transmitted pressure on the target and the obtained maximum tensile zone within it (Section 5). The transmitted pressure is increasing with the increasing the acoustical impedance of the target comparing to Pure Al which consists the top layer of the Al tape. Where 20% gain in the transmitted pressure can be obtained when the substrate is Inconel-718 comparing to the pressure arrived on the Pure Al substrate as shown in Fig. 9a. This transmitted pressure is sensitive also to the acrylic thickness in the Al tape, where for big thickness some attenuation occurred as has been demonstrated in Fig. 9b. The drop in the transmitted pressure is caused by the propagation of the pressure loading release and its reflection in the layer which is higher in the case of Inconel-718 because of its higher acoustical impedance.

In addition, maximum tensile zone has been identified in the 1 mm Pure Al taped target subjected to laser shock. The increase of the acrylic thickness in the Al tape part is leading to decrease in the maximum tensile stress but giving more localized stress and close to the front face, as the one of 200 μm in Fig. 10f. Nonetheless, at the same location using 26 μm of acrylic 1.34 GPa as tensile stress has been obtained, but the maximum tensile stress value is of 1.48 GPa, which has been located close to the back face. So the acrylic thickness could be adjusted to optimize the localization of the maximum tensile zone, and the drop in the stress values due to the attenuation could be compensated by the increase of the energy. To compensate this drop, 2.5 GW/cm^2 laser intensity is enough to obtain the same tensile stress of 1.34 GPa at 250 μm in the 1 mm Pure Al target but with advantage of localized stress zone.

7. Conclusion and outlook

In this study, the validated numerical model of the Al tape has been provided which can be used to optimize laser shock process (LSP, LASAT, LPSP). By coupling experimental and numerical approaches, the capability of laser shock to characterizes the glassy behavior of polymers under high strain rate of deformation (order of 10^6 s^{-1}) has been proved. By changing the substrate and due to impedance mismatch, transmitted pressure could be bigger than the applied one. The maximum tensile zone has been found close to the front face using always one laser beam on thick acrylic layer in the Al tape. The conditions of debonded tape should be taken into consideration, specially in case of overlapping for LSPP process. The validated methodology could be used to model polymers under high strain rate of deformation, and the validated models can also serve as the potential candidate in optimizing laser shock process.

CRediT authorship contribution statement

M. Ayad: Methodology, Writing, Simulation, Experiments. **S. Ünaldi:** Experiments, Methodology, Writing. **M. Scius-Bertrand:** Experiments, Writing. **C. Le Bras:** Experiments. **B. Fayolle:** Investigation, Writing. **L. Berthe:** Writing – review & editing, Project administration, Methodology.

Data availability

Data will be made available on request.

Acknowledgments

This work was supported by Direction Générale de l'Armement (DGA) Rapid during Vanesses project. This project also has received funding from the Clean Sky 2 Joint Undertaking under the European Union's Horizon 2020 research and innovation programme. The authors acknowledge the company DynaS+ for their numerical and simulation supports. The authors acknowledge Simon Bardy and Romain Ecault for their scientific discussions and ideas.

References

[1] K. Langer, T.J. Spradlin, M.E. Fitzpatrick, Finite element analysis of laser peening of thin aluminum structures, Metals 10 (2020) http://dx.doi.org/10.3390/met10010093.
[2] B. Wu, Y.C. Shin, A self-closed thermal model for laser shock peening under the water confinement regime configuration and comparisons to experiments, J. Appl. Phys. 97 (2005) http://dx.doi.org/10.1063/1.1915537.
[3] Y. Liao, C. Ye, B.-J. Kim, S. Suslov, E.A. Stach, G.J. Cheng, Nucleation of highly dense nanoscale precipitates based on warm laser shock peening, J. Appl. Phys. 108 (2010) http://dx.doi.org/10.1063/1.3481858.
[4] C. Ye, S. Suslov, D. Lin, Y. Liao, X. Fei, G.J. Cheng, Microstructure and mechanical properties of copper subjected to cryogenic laser shock peening, J. Appl. Phys. 110 (2011) http://dx.doi.org/10.1063/1.3651508.
[5] U. Trdan, J. Grum, Evaluation of corrosion resistance of aa6082-t651 aluminium alloy after laser shock peening by means of cyclic polarisation and els methods, Corros. Sci. 59 (2012) 324–333, http://dx.doi.org/10.1016/j.corsci.2012.03.019.
[6] U. Trdan, J. Grum, Sem/eds characterization of laser shock peening effect on localized corrosion of al alloy in a near natural chloride environment, Corros. Sci. 82 (2014) 328–338, http://dx.doi.org/10.1016/j.corsci.2014.01.032.
[7] U. Trdan, T. Sano, D. Klobčar, Y. Sano, J. Grum, R. Šturm, Improvement of corrosion resistance of aa2024-t3 using femtosecond laser peening with out protective and confining medium, Corros. Sci. 143 (2018) 46–55, http://dx.doi.org/10.1016/j.corsci.2018.08.030.
[8] Z. Cao, H. Xu, S. Zou, Z. Che, Investigation of surface integrity on tc17 titanium alloy treated by square-spot laser shock peening, Chin. J. Aeronaut. 25 (4) (2012) 650–656, http://dx.doi.org/10.1016/S1000-9361(11)60429-9.
[9] M. Achintha, D. Nowell, D. Fufari, E. Sackett, M. Bache, Fatigue behaviour of geometric features subjected to laser shock peening: Experiments and modelling, Int. J. Fatigue 62 (2014) 171–179, http://dx.doi.org/10.1016/j.ijfatigue.2013.04.016, 9th Fatigue Damage of Structural Materials Conference.
[10] R. Ecault, F. Touchard, L. Berthe, M. Boustie, Laser shock adhesion test numerical optimization for composite bonding assessment, Compos. Struct. 247 (2020) http://dx.doi.org/10.1016/j.compstruct.2020.112441.
[11] L. Berthe, M. Arrigoni, M. Boustie, J.P. Cuq-Lelandais, C. Broussillou, G. Fabre, M. Jeandin, V. Guipont, M. Nivard, State-of-the-art laser adhesion test (LASAT), Nondestruct. Test. Eval. 26 (3–4) (2011) 303–317, http://dx.doi.org/10.1080/10589759.2011.573550.
[12] R. Ecault, F. Touchard, M. Boustie, L. Berthe, N. Dominguez, Numerical modeling of laser-induced shock experiments for the development of the adhesion test for bonded composite materials, Compos. Struct. 152 (2016) 382–394, http://dx.doi.org/10.1016/j.compstruct.2016.05.032.
[13] S. Ünaldi, K. Papadopoulos, A. Rondepierre, Y. Rouchausse, A. Karanika, F. Deliane, K. Tserpes, G. Floros, E. Richaud, L. Berthe, Towards selective laser paint stripping using shock waves produced by laser-plasma interaction for aeronautical applications on aa 2024 based substrates, Opt. Laser Technol. 141 (2021) http://dx.doi.org/10.1016/j.optlastec.2021.107095.
[14] M. Scius-Bertrand, L. Videau, A. Rondepierre, E. Lescoute, Y. Rouchausse, J. Kaufman, D. Rostohar, J. Brajer, L. Berthe, Laser induced plasma characterization in direct and water confined regimes: New advances in experimental studies and numerical modelling, J. Phys. D: Appl. Phys. 54 (2020) http://dx.doi.org/10.1088/1361-6463/abc040.
[15] S. Bardy, B. Aubert, T. Bergara, L. Berthe, P. Combis, D. Hébert, E. Lescoute, Y. Rouchausse, L. Videau, Development of a numerical code for laser-induced shock waves applications, Opt. Laser Technol. 124 (105983) (2020) 1–12, http://dx.doi.org/10.1016/j.optlastec.2019.105983.
[16] A. Rondepierre, S. Ünaldi, Y. Rouchausse, L. Videau, R. Fabbro, O. Casagrande, C. Simon-Boisson, H. Besaucèle, O. Castelnau, L. Berthe, Beam size dependency of a laser-induced plasma in confined regime: Shortening of the plasma release. Influence on pressure and thermal loading, Opt. Laser Technol. 135 (2021) http://dx.doi.org/10.1016/j.optlastec.2020.106689.
[17] M. Ayad, L. Lapostolle, A. Rondepierre, C. Le Bras, M. Scius-Bertrand, S. Ünaldi, U. Trdan, Y. Rouchausse, J. Grassy, T. Maillot, V. Lapoujade, C. Michel, L. Berthe, Modeling of multi-edge effects in the case of laser shock loadings applied on thin foils: Application for material characterization of aluminum alloys, J. Appl. Phys. 131 (9) (2022) http://dx.doi.org/10.1063/5.0080326.

[18] M. Scius-Bertrand, Endommagements maitrisés par choc laser symétrique et désassemblage des collages (Theses), HESAM Université, 2021, URL https://pastel.archives-ouvertes.fr/tel-03683962.
[19] S. Bovid, M. Kattoura, A. Clauer, A. Vivek, G. Daehn, S. Niezgoda, Pressure amplification and modelization in laser shock peening of ti-6al-4v and aa7085 with adhesive-backed opaque overlays, J. Mater Process. Technol. 299 (2022) http://dx.doi.org/10.1016/j.jmatprotec.2021.117381.
[20] P. Peyre, L. Berthe, X. Scherpereel, R. Fabbro, Laser-shock processing of aluminium-coated 55c1 steel in water-confinement regime, characterization and application to high-cycle fatigue behaviour, J. Mater. Sci. 33 (1998) 1421–1429, http://dx.doi.org/10.1023/A:1004331205389.
[21] X. Hong, S. Wang, D. Guo, H. Wu, J. Wang, Y. Dai, X. Xia, Y. Xie, Confining medium and absorptive overlay: Their effects on a laser-induced+ shock wave, Opt. Lasers Eng. 29 (6) (1998) 447–455, http://dx.doi.org/10.1016/S01438166(98)80012-2.
[22] C. Roland, S. Hensel-Bielowka, M. Paluch, R. Casalini, Supercooled dynamics of glass-forming liquids and polymers under hydrostatic pressure, Rep. Progr. Phys. 68 (6) (2005) 1405.
[23] S. Walley, J. Field, Strain rate sensitivity of polymers in compression from low to high rates, DYMAT J. 1 (3) (1994) 211–227.
[24] A. Mulliken, M. Boyce, Mechanics of the rate-dependent elastic–plastic deformation of glassy polymers from low to high strain rates, Int. J. Solids Struct. 43 (5) (2006) 1331–1356, http://dx.doi.org/10.1016/j.ijsolstr.2005.04.016.
[25] C. Le Bras, C. Fosse, L. Delbreilh, M. Gervais, M. Ayad, A.S. Sounakoye, L. Berthe, S. Valadon, B. Fayolle, Transition of elastomers from a rubber to glassy state under laser shock conditions, Soft Matter (2022) http://dx.doi.org/10.1039/D2SM00056C.
[26] L. Barker, R. Hollenbach, Laser interferometer for measuring high velocities of any reflecting surface, J. Appl. Phys. 43 (11) (1972) 4669–4675.
[27] L. Barker, R. Hollenbach, Shock-wave studies of PMMA, fused silica, and sapphire, J. Appl. Phys. 41 (10) (1970) 4208–4226.
[28] D.J. Steinberg, S.G. Cochran, M.W. Guinan, A constitutive model for metals applicable at high-strain rate, J. Appl. Phys. 51 (3) (1980) 1498–1504, http://dx.doi.org/10.1063/1.327799.
[29] B. O'Toole, M. Trabia, R. Hixson, S.K. Roy, M. Pena, S. Becker, E. Daykin, E. MacHorro, R. Jennings, M. Matthes, Modeling plastic deformation of steel plates in hypervelocity impact experiments, Procedia Eng. 103 (December) (2015) 458–465, http://dx.doi.org/10.1016/j.proeng.2015.04.060.
[30] J. López-Puente, A. Arias, R. Zaera, C. Navarro, The effect of the thickness of the adhesive layer on the ballistic limit of ceramic/metal armours. an experimental and numerical study, Int. J. Impact Eng. 32 (1) (2005) 321–336, http://dx.doi.org/10.1016/j.ijimpeng.2005.07.014, Fifth International Symposium on Impact Engineering.
[31] J.C. Boettger, Sesame Equation of State for Epoxy, Tech. Rep., Los Alamos national laboratory, 1994, http://dx.doi.org/10.2172/10131920.
[32] Online materials information resource-matweb, 2021, http://www.matweb.com. (Accessed 23 March 2021).
[33] J.E. Mark, Physical Properties of Polymers HandBook, Springer New York, NY, 2007.
[34] D.W. Van Krevelen, K. Te Nijenhuis, Properties of Polymers: Their Correlation with Chemical Structure; their Numerical Estimation and Prediction from Additive Group Contributions, Elsevier, 2009.
[35] H.K. Farahani, M. Ketabchi, S. Zangeneh, Determination of Johnson–Cook plasticity model parameters for Inconel718, J. Mater. Eng. Perform. 26 (11) (2017) 5284–5293, http://dx.doi.org/10.1007/s11665-017-2990-2.